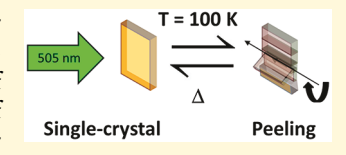


Light-Induced Macroscopic Peeling of Single Crystal Driven by **Photoisomeric Nano-Optical Switching**

Jacqueline M. Cole,*,†,‡,\$,|| Dose de J. Velazquez-Garcia,† David J. Gosztola, SuYin Grass Wang, and Yu-Sheng Chen¹

Supporting Information

ABSTRACT: Single-crystal optical actuators are emerging as a prospective material form for nano-optical mechanical switching, sensing, or transduction device applications in nanotechnology and quantum technology. Crystal-lattice strain effects lie at the molecular origins of their macroscopic optical behavior, and linkage photoisomerization is an attractive source of optical actuation, if only suitably functioning materials of this ilk could be found. We discover $\eta^{\bar{1}}$ -SO₂ to η^{1} -OSO single-crystal linkage photoisomerization in $[Ru(NH_3)_4(SO_2)(3-1)]$



phenylpyridine)]Cl2·H2O, which behaves macroscopically as a single-crystal optical actuator, whereby the crystal peels in response to light-induction at 100 K. It thermally recovers, whereupon the crystal exhibits remarkable restorative properties. We apply photocrystallography alongside concerted optical microscopy and optical absorption spectroscopy to reveal how the molecular origins of photoisomerization induce crystal-lattice strain that engenders this macroscopic crystal peeling effect. Linking structure and function across molecular and macroscopic length scales showcases a means by which single-crystal optically actuating materials could be systematically designed.

■ INTRODUCTION

Crystals have long been held as rigid and static forms of materials, due to their highly regularized and periodic lattice frameworks of ordered molecules. Out-of-equilibrium phenomena can nonetheless exist within the crystalline state when they are driven by an external stimulus. Such phenomena often engender the function of a material, while the ordered nature of single crystals offers high consistency in fabrication if they could operate as actual devices. Learning how to control outof-equilibrium phenomena within single crystals that can act as devices thus presents an enormous opportunity for functional materials science. Single-crystal optical actuators are emerging as candidates for key applications in nanotechnology^{1,2} and quantum-technology,3 due to their function as nano-optical switches, sensors, or transducers, especially where they can be used to create a macroscopic mechanical motion.

Single-crystal optical actuators are being found that display a variety of macroscopic responses to light-stimuli: 4 bending, twisting, coiling, jumping, creeping, and exploding. These are all forms of elastic or plastic deformation. Most of these actuators discovered to date are the result of photoinduced chemical reactions that can occur within single crystals; the chemical product is realized via a light-induced structural transformation within the crystal lattice, building up strain that is typically alleviated by a mechanical response. 5-12 While some of these reactions are reversible, the strain induced causes many crystals to explode. Moreover, most of these case studies are organic materials, whose limited thermal stability has presented major historical issues for practical applications in the wider field of photonics.¹³ Metal-organic complexes offer much better thermal stability while retaining their organic versatility. Certain metal-organic complexes can exhibit linkage photoisomerism, which operates via a nano-optical switching mechanism.¹⁴ This could provide a route to singlecrystal optical actuation. Additionally, its intramolecular origins make it particularly attractive to device technology: for example, it is more controllable and requires less energy than intermolecular reactions. That said, the material, [Co-(NH₃)₅(NO₂)]Cl(NO₃), appears to stand alone in reports that demonstrate both single-crystal linkage photoisomerism¹⁵ and single-crystal optical actuation. 16 While these reports acknowledge that crystal-lattice strain at the molecular level must govern their macroscopically observed optical actuation,

Received: May 3, 2019 Revised: June 11, 2019 Published: June 11, 2019

[†]Cavendish Laboratory, Department of Physics, University of Cambridge, I. J. Thomson Avenue, Cambridge CB3 0HE, United Kingdom

[‡]ISIS Neutron and Muon Source, STFC Rutherford Appleton Laboratory, Harwell Science and Innovation Campus, Didcot, Oxfordshire OX11 0QX, United Kingdom

Department of Chemical Engineering and Biotechnology, University of Cambridge, West Cambridge Site, Philippa Fawcett Drive, Cambridge CB3 0AS, United Kingdom

Argonne National Laboratory, 9700 South Cass Avenue, Lemont, Illinois 60439, United States

[⊥]NSF's ChemMatCARS Beamline, The University of Chicago, Advanced Photon Source, Lemont, Illinois 60439, United States

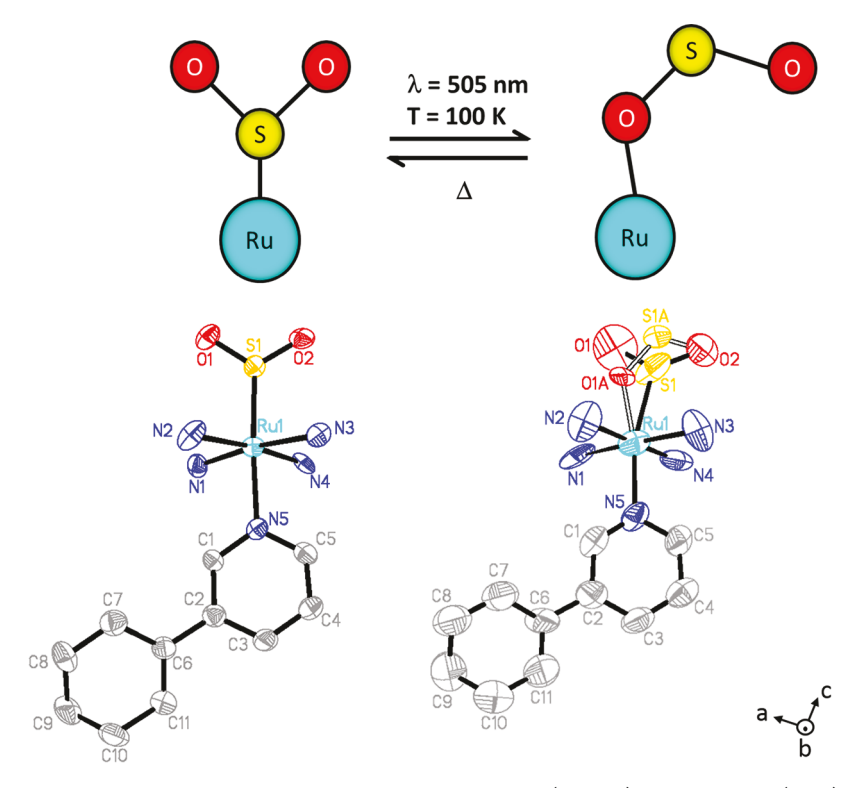


Figure 1. (top) Schematic of the linkage photoisomerization process observed in 1. (bottom) Light-induced (right) and dark-state (left) crystal structures of 1 at 100 K, showing anisotropic displacement parameters at the 50% probability level. The η^1 -OSO photoisomer is shown with hollow-bonds, while the η^1 -SO₂ ligand configuration is presented with solid-bonds. Hydrogen atoms, chloride ions, and the water of crystallization are omitted for clarity.

they state that its molecular characterization was compromised heavily by the tendency of its crystals to fracture.

In this study, we showcase the discovery of a new singlecrystal optical actuator, [Ru(NH₃)₄(SO₂)(3-phenylpyridine)]-Cl₂·H₂O (1), whose mechanism is governed by single-crystal linkage photoisomerism. Crucially, we enable an intrinsic link between its macroscopically observed optical phenomenon and its molecular origins by coupling concerted optical microscopy and absorption spectroscopy with a light-induced in situ singlecrystal X-ray diffraction study. Creating this link is incredibly important, because it lays a foundation for a systematic approach to the molecular design of single-crystal optical actuators. The dark- and light-induced crystal structures of 1 were captured using in situ photostimulated single-crystal Xray diffraction at 100 K. These structures reveal the nanooptical switching, which is caused by η^1 -SO₂ to η^1 -OSO linkage photoisomerization. We then demonstrate how this lightinduced structural change results in the macroscopic peeling of a single crystal of 1 at 100 K, using a custom-built concerted optical absorption microscopy and spectroscopy setup with N₂ cryogenic capabilities. We observe that this crystal peeling effect is thermally reversible to the extent that it shows remarkable restorative properties upon warming to room temperature. Pseudomerohedral twinning appears to be crucial to this light-induced macroscopic crystal motion, whose mechanism tracks a five-step process: (i) SO₂ linkage photoisomerization, which (ii) builds up crystal-lattice strain, that (iii) is alleviated by crystal buckling, which (iv) enables further optical absorption and photoisomerization, that, in turn, (v) yields a compensatory curling effect.

■ RESULTS AND DISCUSSION

The solid-state η^1 -SO₂ to η^1 -OSO linkage photoisomerization that affords the single-crystal nano-optical switching phenomenon in 1 is illustrated in Figure 1. The most thermally stable S-bound η^1 -SO₂ ligand configuration (Figure 1, top left) is generally expected for SO₂ ligand coordination, as is represented by our dark-state crystal structure determination of 1 (Figure 1, bottom left). These crystallographic data were obtained from a $120 \times 30 \times 5 \mu \text{m}^3$ crystal, held at 100 K, using synchrotron-based single-crystal X-ray diffraction at the NSF's ChemMatCars beamline of the Advanced Photon Source, U.S. The light-induced crystal structure of 1 (Figure 1, right) was then deduced by applying green light ($\lambda = 505$ nm) to this crystal for 2.5 h, while holding its diffractometer position and temperature at 100 K, and then acquiring and processing an otherwise identical data set. Details of this developing in situ light-stimulated single-crystal X-ray diffraction method, becoming known as photocrystallography, are described elsewhere 17-20 and in the Supporting Information. 52(3)% of the SO₂ ligands in the crystal lattice of 1 were found to photoconvert to an O-bound η^1 -OSO configuration, as indicated by the hollow-bonded SO₂ ligand coordinated to ruthenium in light-induced crystal structure of 1 (Figure 1, bottom right). Its residual 48(3)% dark-state SO₂ component (solid-bonded SO₂ ligand shown in Figure 1, bottom right) is tilted slightly to accommodate this linkage photoisomerism.

In common with other nano-optical switching ruthenium-based sulfur dioxide ammine (hereafter denoted [Ru–SO $_2$]) complexes, $^{21-29}$ this light-induced structure of 1 exists as a metastable state at 100 K, and reverts to its dark-state crystal structure once warmed to room temperature. However, the nano-optical switching of 1 is distinctly untypical for this family

of ruthenium-based complexes, in that it only presents with the η^1 -OSO photoisomer; all other reports on [Ru-SO₂] complexes manifest a S-O side-bound η^2 -SO₂ type of photoisomerization^{21,22,24} tion^{21,22,24} or a mix of that with some η^1 -OSO photo-isomerization. Moreover, the 52(3)% η^1 -OSO photoconversion fraction in 1 is the highest observed in all [Ru-SO₂] complexes reported to date. This stands to reason considering both steric and chemical characteristics of the 3phenylpyridine trans ligand in 1. 3-Phenylpyridine affords the largest steric contribution of any 3-substituted pyridine trans ligand in photocrystallographically reported [Ru(SO₂)] complexes. In terms of chemical properties, the nitrogen atom in 3phenylpyridine possesses the second largest p K_a value (4.73)³⁰ of any 3-substituted pyridine ligand in these [Ru(SO₂)] structures. The largest pK_a value of a trans ligand in reported $[Ru(SO_2)]$ crystal structures belongs to 3-pyridine (pK_3) 5.12), whose $[Ru(SO_2)(NH_3)_4(3-pyridine)]Cl_2 \cdot H_2O$ photocrystallographic structural counterpart to 1 displayed the largest η^1 -OSO photoconversion fraction (44.5(7)%) until now,²⁹ given the report herein on 1 with 52(3)%.

1 crystallizes as a pseudomerohedral twin, where librational disorder of the phenyl group in its 3-phenylpyridine ligand confines the space-group symmetry to P2₁ (see Supporting Information). The unit cell dimensions of 1 change substantially upon photoconversion, whereby all unit cell lengths change by $\sim 1\%$ while β changes by 2% (see Table S4). β subtends the a,c-crystallographic plane, in which all of the bond-geometry changes of the SO₂ photoisomerization effect occur (see Figure S1). The unit cell length that changes most upon photoconversion is c, to which the η^1 -S_{bound}-Ru-N_{pyridyl} axis is primarily aligned; this axis hosts the largest light-induced bond-length changes in 1, with Ru1-N5 (dark) 2.119(4) Å; Ru1-N5 (light) 2.062(8) Å; that is, Δ (Ru-N_{pyridyl}) = 1.3%, and Ru1-S1 2.1173(14) Å; Ru1-S1 (light) 2.22(2) Å; that is, Δ (S_{bound}-Ru) = 4.9% (see Table S5 for more details about light-induced changes in the Ru-coordination geometry). The fact that these particularly large bond-geometry changes occur along this S-Ru-N axis stands to reason, considering the substantial trans influence that is expected to manifest in 1 due to the large pK_a value of 3-phenylpyridine, which, in turn, explains the large SO₂ photoconversion fraction.^{26,2}

The macroscopic manifestation of this nano-optical switching phenomenon in single crystals of 1 was studied via low-temperature optical microscopy. This apparatus formed part of a custom-built concerted optical microscopy and absorption spectroscopy setup with an optics bench to deliver controlled incident green light to a single crystal that was housed inside an optical cryostat with temperature control. Further details are given in the Supporting Information, as are full movies of the various optical microscopy time sequences discussed below, while only selected frames are presented in Figures 2 and 3.

Figure 2 (top panel) shows how a single crystal of 1 responds to t minutes of stimulation by green (λ = 505 nm) light while held at 100 K. The time sequence shows a remarkable crystal "peeling" effect that begins with the light-induced lateral cut in the crystal seen at the t = 20 min snapshot, and spans through to t = 1600 min during which a crystal segment on one side of this cut progressively curls as it continues to be exposed to more light. A progressive darkening of the crystal is associated with this light-induced effect. Such photochromic changes are commonly observed in $[Ru-SO_2]$ complexes, while this macroscopic crystal "peeling" effect is



Figure 2. (top panel) Eight optical microscopy snapshots of a movie that illustrates the crystal peeling as a response to t minutes of its first cycle of light induction ($\lambda=505$ nm) at T=100 K. A photochromic change from orange to deep blue is shown, which is caused by an associated linkage photoisomerization effect. (bottom panel) Eight optical microscopy snapshots of a movie that demonstrates the partial thermal recovery of the crystal whereby the peeling is largely reversed as the crystal is warmed to temperature, T. A crystal buckling effect that initiated this crystal peeling effect is apparent in these images. See movie S1 for further illustration.

unprecedented. Dark lines can be seen in the lateral sections inside the cut at the higher time regimes; for example, there are two intensely dark lateral lines inside the cut at t = 1600 min, at the time when the peeling has finally extended as far as it can

This light-induced structural effect in 1 was then reversed by warming the crystal to room temperature. Figure 2 (bottom panel) shows that the crystal reverts to its original color within a temperature rise of 70 K, as is fairly typical for the thermal decay of an η^1 -OSO photoisomer in [Ru-SO₂] complexes; the exact decay lifetime depends on the warming rate, which in our case was 1.5 K/5 s within the 100-200 K temperature elevation stage. The photochromic (and thus photoisomeric) reversion occurs before the crystal peeling effect has subsided. The increase in transparency of the crystal reveals that the light-induced cut is actually caused by a buckling effect, cf., the raised crystal sections on either side of the cut, which gradually close in synchrony much like the operation of a two-sided drawbridge. This closure occurs as a function of increasing temperature, but primarily during 230-250 K, which corresponds precisely to the temperature range in which a heavy drop in viscosity is observed for the perfluoroether oil that holds the crystal frozen on a sapphire disk within the optical cryostat. Thus, a physical "clamping" effect is apparent, and seems to trap this macroscopic crystal peeling phenomenon, long after the photoisomer has decayed; this finding bears striking parallels to crystal clamping effects observed in many types of phase transitions and mode softening phenomena. Notice that the cut does not fully close



Figure 3. (top panel) Eight optical microscopy snapshots of a movie that illustrates the warming effect during a second cycle of lightinduction (albeit for only t = 30 min) followed by heating to room temperature. The images show how the crystal peeling effect fully recovers upon warming as the crystal cut closes completely. (bottom panel) Two pairs of four optical microscopy snapshots of a movie, which illustrate respectively the first and second parts of a third cycle of crystal light-induction (albeit for only t = 90 min) followed by warming to room temperature. These time sequences show how the crystal has restored itself to the extent that its residual domain line does not reopen upon application of light; instead, other domain lines form to accommodate the light-induced crystal strain. The domain line residing from the crystal restorative process appears to be no more susceptible than the other domain lines toward crystal buckling. See movie S2 and movie S3 for further illustration of cycles 2 and 3, respectively.

and the lines from the "drawbridge hinges" remain in the crystal, even after it reaches room temperature.

Figure 3 (top panel) demonstrates quite remarkably that the cut can nonetheless be fully closed by repeating the light-induction (albeit for only 30 min) and warming cycle. The corresponding time sequence upon warming reproduces the same trend that was tracked in Figure 2 in that the drawbridge closes primarily between 230 and 250 K, but with the stark exception that the cut closes much more tightly, such that the two sides of the drawbridge are seen to touch in the photo marked with T=246 K. The next photo (T=249 K) shows that the right-hand drawbridge hinge has disappeared, and a thick dark line rests in place of the cut. This dark line moves closer to the left-hand hinge line upon warming to T=271 K, and appears much thinner.

Figure 3 (bottom panel) presents a third cycle of inducing light and warming the crystal. Four time snapshots that span 90 min of light induction first reveal that, while the dark line that resides from the cut location becomes thicker, it does not reopen. Rather, a series of other dark lines form laterally across the crystal, perhaps best seen at the t=37 min snapshot before the crystal becomes as dark as it can be by only 90 min of light induction, judging from the darkness achieved by the other

light-induced cycles. The line pertaining to the original cut location is no thicker than many of these lines, indicating that it is no more vulnerable than some of the other lines in being the point of crystal buckling. In other words, the crystal appears to have sufficiently restored its crystal forces within this domain line that it has essentially healed itself. The third cycle of crystal warming (Figure 3, bottom panel) suggests that these many lateral lines all result from the same type of light-induced crystal-lattice strain that was previously alleviated by the crystal peeling effect, by virtue of the fact that these lines dissipate in the same temperature region where the crystal stops being frozen to its substrate (240–250 K).

Simultaneous optical absorption spectroscopy was performed alongside these optical microscopy studies, because photoisomerization changes can be inferred indirectly from various modulations in metal-ligand charge-transfer (MLCT) that manifest as changes in optical absorption. While our single-crystal X-ray diffraction studies have provided a 3-D representation and quantitative measure of photoisomerization, photocrystallography is a bulk technique; it therefore becomes of limited use once a crystal begins to peel. In contrast, optical absorption spectroscopy can measure time sequences of optical absorption at highly localized points in a crystal. This is very poignant to this study where we wish to understand the correlated structural and optical absorption changes inside and outside of the cut observed in the crystal, where there exists a distinct optical absorption gradient. Indeed, the optical microscopy shows that the crystal is more transparent inside the cut, relative to that of its exterior surface, as we saw in Figure 2. The exposure of the crystal interior engendered by this cut thus allows light to penetrate deeper into the crystal such that it absorbs more light. Light must nonetheless pass through the entire crystal; otherwise the crystal would not be observed by optical microscopy or spectroscopy as it operates in transmission mode.

Accordingly, the optical absorption spectra shown in Figure 4 were collected on the crystal at two locations: one outside the cut and one inside the cut, as indicated by the white circles in the crystal overlays. These spectra relay the time series of optical absorption changes that occur during the first cycle of light-induction, which were measured in tandem with the optical microscopy images shown in Figure 2. Note that the crystal suddenly absorbs more red light at t = 20 min, which quickly dissipates at both crystal locations shown; this is presumably caused by the newly exposed surface inside the cut adjusting to a change in optical absorption with respect to the deeper interior of the crystal. The optical absorption of the crystal at both locations then recovers and thereafter increases monotonically, while their respective overarching spectral profiles remain essentially constant. By t = 80 min, the absorption has plateaued, rendering the crystal region outside the cut as a blackbody for visible light, while the region inside the cut retains a dip in optical absorption between 500 and 600 nm, affording it a deep blue hue. The optical densities inside and outside of the cut remain different throughout this time sequence, as is expected given the thinner crystal cross-section associated with the measurements within the cut.

This difference in optical density will induce a particularly acute absorption contrast at the point of the crystal buckling hinge; indeed, careful observation of this region in Figure 2 (top panel) reveals a bright line that tracks the intersection of the right-hand hinge with the inside of the cut, as the hinge moves along the crystal face. There will presumably be a

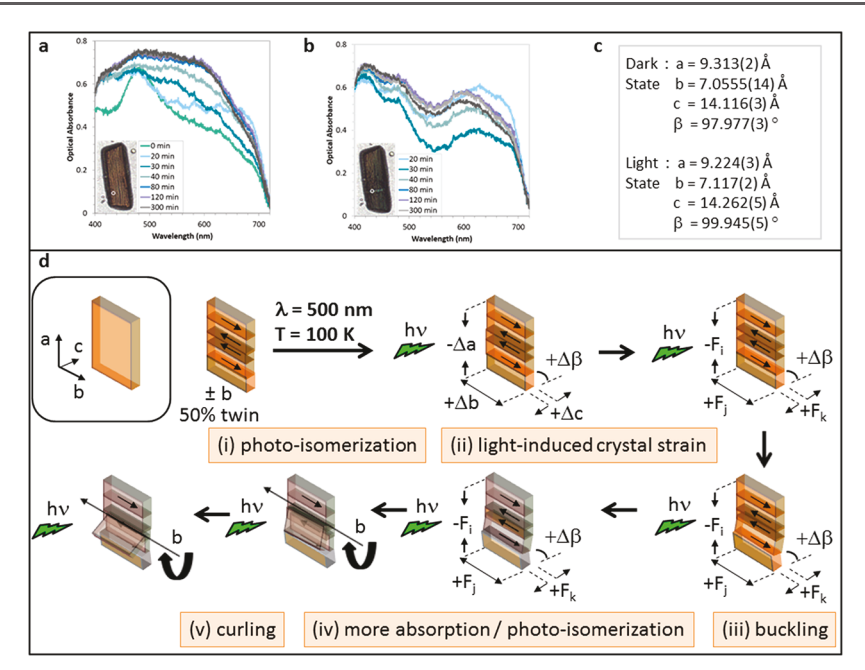


Figure 4. (a) Single-crystal optical absorption spectra of 1 at 100 K acquired during the first cycle of the light-induction process in concert with the optical microscopy images illustrated in Figure 2. The optical microscopy overlay in each spectrum carries a white circle that pinpoints the location on the crystal that the optical absorption spectrum probed, that is, (a) outside and (b) inside the light-induced crystal cut. (c) The unit cell parameters of the dark- and light-induced crystal structure of 1. (d, inset) The orientation of the crystal with respect to these unit cell parameters. (d) The five-step mechanism by which a pseudomerohedral twinned crystal of 1 undergoes (i) η^1 -SO₂ to η^1 -OSO linkage photoisomerization whose changes in unit cell parameters present the buildup of (ii) light-induced crystal strain, which results in a (iii) crystal buckling effect to alleviate this strain, that affords a cut in the crystal surface into which (iv) more light absorbs, which enables more linkage photoisomerization that in turn produces a compensatory (v) crystal curling effect. The overall mechanism represents a macroscopic crystal peeling effect, which is nonetheless linked to its nano-optical switching origins at the molecular scale.

commensurate photoisomerization contrast in the region of this hinge. Because an increase in optical absorption tends to be correlated with an increase in levels of photoisomerization, the hinge will likely open to alleviate the light-induced crystal strain caused by this contrast. The hinge opens via a curling effect that lessens with increasing light-induction, becoming barely discernible above t=80 min where the optical absorption has plateaued.

We now propose a five-step mechanism that relates the nano-optical switching effect to the observed macroscopic crystal peeling behavior. Figure 4 (boxed image, middle, left) shows how the crystal habit of the sample displayed in Figures 2 and 3 is oriented with respect to its crystallographic axes; the ability to map the axes associated with these nanoscopic and macroscopic effects is a prerequisite to uncovering the peeling mechanism. The twinned nature of the crystal obscures a precise determination of the Miller index associated with its large crystal face, although it was judged to be close, if not identical, to a (001) plane. Figure 4 (bottom half) shows that the pseudomerohedral twinning of 1 is a necessary starting point for this mechanism, given that it requires crystal domains, which differ by a reversal of the crystallographic baxis. The $\pm b$ variation that results from the pseudomerohedral twinning of 1 thus engenders twin boundaries that align with the photoinduced domain lines observed laterally across the crystal.

The external light (λ = 505 nm) associated with the photoisomerization (Figure 4, step i) lies incident to the normal of the large crystal face, which undergoes optical absorption at 100 K. Given our earlier note that the photocrystallographic structure of 1 features SO₂ photo-

isomerization contained within the a,c-crystallographic plane and that the largest bond-geometry changes are directed along c, this external green light will pass along the direction of maximum light-induced structural change. Accordingly, light-induced crystal-lattice strain builds up in the crystal as it progressively absorbs this green light and thus engenders more SO_2 photoisomers. The anisotropic nature of this strain can be inferred by the cell parameters of the dark- and light-induced crystal structures (Figure 4, top right). These show that the SO_2 linkage photoisomerization causes the b- and c-crystallographic planes to expand and the angle between the a,c-plane (β) to extend, while the crystallographic a-axis contracts. These changes and associated forces are depicted in step ii of Figure 4.

The photocrystallographic results showed that the percentage change in β observed upon photostimulation is about double that of any of the unit cell axes (cf., 1% changes in a, b, or c versus a 2% change in β). The competing effects of the contracting a-axis against the expansion of all of the other cell parameters cause the crystal to buckle between the *b,c*-planes. The twin boundaries that lie along b present natural weak domain walls to enable this crystal buckling process; this is represented by step iii of Figure 4. The cut in the crystal created by this buckling effect permits more light to penetrate deeper into the crystal. This increases its optical absorption and thence photoisomerization levels (Figure 4, step iv), as indicated by the optical spectra (Figure 4, top) whose absorption continues to change until about 80 min of light induction. An absorption contrast builds up between the two crystal surfaces that are exposed to the light, wherein the hinge of the crystal buckling effect is particularly susceptible to the

associated light-induced crystal strain. The hinge opens in response via a curling action (Figure 4, step v).

The observation that this motion response is a curling effect, rather than another type of macroscopic response, appears to be a result of various nanoscopic origins. It is no coincidence that $\Delta \beta$ involves a rotation whose unique crystallographic baxis lies precisely along the axis of the curling motion observed. The crystal symmetry of 1 is also relevant in that $\Delta\beta$ relates to commensurate changes in the a,c-crystallographic plane, in which the SO₂ photoisomerization effects are contained; a corollary is that the curling behavior effectively accommodates the spatial changes caused by SO₂ photoisomerization effects. The peeling phenomenon will also act in response to the largest bond changes in 1 that are associated with the SO2 photoisomerization effect; these concern the significant geometric perturbation in Ru-coordination, along its S-Ru-N axis, which aligns close to the direction of the crystallographic axis, c, that is, normal to the crystal face that peels. Presumably, this curling effect will also alleviate the librational disorder of the 3-phenylpyridine that engenders motion in this peeling direction (see Figure S1).

Eventually, light-induced crystal strain appears to impose a limit on the extent of curling, judging from the movies in the Supporting Information, which indicate a progressive halting of the peeling effect, as the strain lines increase in strength and number. Once a sufficient amount of crystal strain has built up, no amount of additional incident light will force the crystal to peel further, as was shown in Figure 2, whereby peeling barely extended beyond 300 min of light-induction and by t=1600 min the crystal was entirely stationary. Thus, the η^1 -OSO photoconversion fraction in 1 would appear to have an upper bound. Overall, this series of forces and motions afford the macroscopic crystal peeling effect observed.

The crystal appears to return to its original state via the reverse procedure with a few exceptions: The external stimulus is heat rather than light. Its optical absorption drops quickly with rising temperature, as the O-bound η^1 -OSO photoisomer reverts to its more thermally stable S-bound η^1 -SO₂ dark-state ligand configuration. The peeling effect (buckling and curling) remains long after the photoisomer has disappeared, due to the aforementioned clamping effects; these render a substantial level of residual strain in the crystal, until the oil used to freeze the crystal on the substrate within the optical cryostat melts. The crystal buckling does not fully reverse until a second cycle of light- and heat-induction, whereupon the two sides of its "drawbridge" become sufficiently close that the crystal lattice can reform. The restorative effect of this crystal provides key insights into the mechanistic forces that govern its molecular origins. In particular, it suggests that the crystal lattice forces are sufficiently strong that they pull the crystal together, to the extent that crystal region associated with the original lightinduced cut is no weaker than the rest of the crystal upon a third cycle of light induction; cf., many strain lines build up in cycle 3 of light-induction, but the crystal is not cut by light (see movie S3). The restorative nature of these photoinduced crystal actuators bears strong parallels to restorative effects that have been observed in thermally and mechanically stimulated crystals.34-36

Tests for reproducibility were also performed, whereby a second crystal of 1 was photoexcited with $\lambda = 505$ nm at 100 K, and monitored by optical microscopy over three cycles of light-induction and warming. The optical microscopy employed the same experimental setup as for the first crystal,

except that a 20× objective (0.40 NA, Olympus, UMPLlanF1) was used for cycles 2 and 3 for this second crystal, whose starting dimensions were $0.350 \times 0.050 \times 0.010 \text{ mm}^3$. The peeling effect was reproduced in this second crystal through all three cycles of investigation, as illustrated via movies S4-S6. The peeling effect in this crystal emanates from one end of the crystal, which, together with its extended length, facilitates a clear visualization of the associated light-induced crystal strain lines; these manifest as dark lateral lines on the main crystal face or as actual optical cuts through the crystal, and appear to form stepwise along the crystal as they increase in number, in response to more light being applied to the crystal. The much larger aspect ratio of the second crystal (35:5 = 7.00) as compared to the main subject crystal (19:7 = 2.71) enables the formation of a much longer chain of strain lines that act to progressively temper and eventually halt the crystal peeling effect. Thus, it stands to reason that the peeling effect in this second crystal does not extend as far as that observed in the main subject crystal. Its more modest extension is perhaps, in turn, a reason why the peeling effect can cycle at least three times in the second crystal, while the main subject crystal was so tempered by the cyclical buildup of light-induced crystal strain lines that it had restored itself and fully halted any further peeling effect after two cycles of light and heat. Indeed, a fourth cycle of light-induction and warming on the main subject crystal was performed 6 months after the original three cycles of experiments, and the results were a replica of its cycle 3 (see movie S7).

A complete interpretation of this phenomenon may not be as simple as considering strain-induced tempering versus crystal peeling effects, because the extent of thermally induced restorative effects of the crystal will also influence the ability of a crystal to undergo light-induced crystal strain and peeling behavior. The second crystal continues to peel across three cycles, and appears to attempt to restore itself given the general reversal of the light-induced peeling upon warming. However, an underlayer of the second crystal slips significantly during the warming phase of cycle 1 (see movie S4), which precludes the crystal from ever fully restoring itself; the physical mismatch in layers persists over cycles 2 and 3, and the crystal fractures in a few places during its pursuit to thermally recover. Despite the progressive deterioration of the crystal, it maintains its ability to peel over at least the three cycles studied, and the peeling effect appears to be essentially elastic in origin. Such origins of force can be compared to those from recent studies on elastic³⁷ and plastic³⁸ bending effects in crystals.

Thermal energy appears to compensate for the more modest light-induced peeling effect that is observed in the second crystal due to its greater light-induced crystal strain. Thermal energy releases some of this crystal strain upon warming such that the initial warming phase of the second crystal actually raises the extent of peeling in the region 135 \pm 10 K < T < 165 \pm 10 K, whereupon it reaches its maximum peeling limit. It is noteworthy that the temperature onset of this further peeling corresponds to the temperature at which η^1 -OSO photoisomers observed in [Ru-SO₂] complexes start to decay into a more thermally robust, metastable, side-bound η^2 -SO₂ configuration ($T \approx 120-130$ K). The crystal maintains this maximum extent of peeling upon further warming until about $T = 215 \pm 5$ K where it starts to curl down as far as it can within the physical constraint of the frozen oil that holds the crystal on the sapphire substrate within the cryostat. This temperature aligns with the typical temperature range, T =

200–220 K, ^{27,29} whereby the side-bound η^2 -SO₂ isomer thermally decays back to its dark-state η^1 -SO₂ configuration. This physical "clamping" effect is overcome once the oil melts at $T=230-240\pm5$ K, whereupon the peeling effect curls down fully as the crystal settles into a stationary state as it continues to warm to room temperature. These distinct warming phases are present in the light and warming cycles 1 and 2 for the main subject crystal but are much more subtle in their manifestation, cf., movie S1 and movie S2. The good and consistent match between these temperature-dependent curling effects and well-known temperature-dependent curling effects and well-known temperature-dependent η^1 -OSO $\to \eta^2$ -SO₂ $\to \eta^1$ -SO₂ linkage isomer conversions in [Ru–SO₂] complexes is particularly compelling evidence to corroborate the relationship between the macroscopic peeling effect in 1 and its nano-optical switching origins.

Overall, there is good reproducibility and consistency between the optical microscopy results for the two crystals studied, and, where differences occur, these can be rationalized and offer further insights into the mechanistic behavior of the crystal peeling effect. One difference worth highlighting is that the aspect ratio of the crystal appears to affect the precise nature and extent of the crystal strain and peeling behavior of 1. An optical microscopy study of many crystals that span a large range of aspect ratios is needed to establish detailed relationships between the strain, peeling, thermal recovery, and restorative characteristics of the crystal. A prerequisite for such a study would be an extensive exploration of crystal growth mechanisms of 1 to furnish a set of new crystals that possess many different types of crystal habits with a large range of disparate aspect ratios for investigation. Establishing such relationships is beyond the scope of this work, but their projected realization could eventually enable the characteristics of this peeling effect to become tunable. This leads to the ultimate goal of tailoring these light-induced optical actuators to suit a given nano-optical switching application.

CONCLUSIONS

In summary, we have discovered a new material that undergoes a light-induced structural change in its single-crystal form, and demonstrated a relationship between its nano-optical switching effect and its macroscopic behavior to light. The field of single-crystal optical actuators is still in its infancy, but our showcasing of structure—function relationships in 1 across the molecular and macroscopic length scales stands to be transformative, in terms of showcasing to this field a means for creating crystalline materials with opto-mechanical function. This argument is especially pertinent when we consider the enormous prospects of these types of single crystals as actual device media, to meet the timely need for mechanically responsive nano-optical switches, sensors, and transducers.

■ EXPERIMENTAL SECTION

Materials. The reaction precursor [Ru(NH₃)₄(SO₂)Cl]Cl was synthesized according to literature methods. All other reagents were purchased from Sigma-Aldrich and used without further purification.

Methods. [Ru(NH₃)₄(SO₂)(3-phenylpyridine)]Cl₂·H₂O (1) was synthesized from a solution of [Ru(NH₃)₄(SO₂)Cl]Cl (5 mg, 16 μ mol) in an aqueous solution of Na₂CO₃ (200 μ L, 1 M), which was mixed with another solution of 3-phenylpyridine (5 μ L, 35 μ mol) in methanol (200 μ L). The resultant mixture immediately turned yellow. Subsequently, hydrochloric acid (100 μ L, 32%) was added dropwise, and orange crystals were formed within 1 h. Finally, the product was recovered by vacuum filtration and washed three times with methanol.

Dark and Photoinduced In Situ Single-Crystal X-ray Diffraction. The crystal structures of the dark- and light-induced states of 1 were determined using synchrotron-based X-ray crystallography, at the NSF's ChemMatCARS beamline of the Advanced Photon Source, Argonne National Laboratory, IL. A $0.120 \times 0.030 \times 0.005$ mm³ single crystal of 1 was mounted onto a Huber three-circle diffractometer equipped with a Pilatus 3 × CdTe 1 M shutterless pixel array detector and a 100 K nitrogen open-flow cryostream delivered by an Oxford cryojet. An X-ray beam of wavelength 0.41328 Å was used to capture a series of data frames over multiple ϕ scans of crystal orientations, collected in 0.3° increments each with 1.0 s exposure time, using five fixed (ω, κ) setups where the diffractometer sat at $(-200^{\circ}, 30^{\circ})$, $(-190^{\circ}, 20^{\circ})$, $(-180^{\circ}, 30^{\circ})$, $(-180^{\circ}, 15^{\circ})$, and $(-180^{\circ}, 0^{\circ})$ respectively, while maintaining a 130 mm sample-to-detector distance. For control purposes, the ambient lighting in the experimental hutch of the beamline was extinguished while data were being acquired for both dark- and light-induced crystal structure determinations. Data for the dark-state crystal structure were first obtained. The crystal was then maintained at 100 K on the diffractometer and rotated continuously while being irradiated with 505 nm light for 2.5 h, using a Thorlabs M505L3 lightemitting diode (LED) whose head power output was 1000 mA constant current and 3.3 V forward voltage. This light was switched off before acquiring data for the light-induced crystal structure. Further experimental details, as well as structure solution and refinement information, are given in the Supporting Information. A more detailed description of the specialized photocrystallography aspects of these experiments is given elsewhere.

Single-Crystal Optical Characterization. A custom-built microspectroscopy system was used to record the absorption spectrum of single crystals under a variety of environmental conditions. The system was built around an inverted microscope (Olympus: IX71) coupled to a 300 mm focal length spectrograph (Princeton Instruments: Acton Series 2300i) and 1320 × 100 channel CCD camera (Princeton Instruments: PIXIS 100BR). A 0.190 × 0.070 × 0.010 mm³ crystal of 1 was mounted on a sapphire disk (9 mm diam, 0.5 mm thick) and fastened with a small amount of viscous perfluoroether oil. The mounted sample was then placed on the coldfinger of an optical cryostat (Janis: ST-500-UC) attached to the microscope. The coldfinger was drilled through, allowing optical absorption measurements to be made. The crystal was positioned such that only one-half of the active vertical channels of the CCD camera were used to image a portion of the crystal using a 10×, 0.13 NA objective (Olympus, NeoSPlan); the remaining one-half of the active detector channels imaged the sapphire substrate. The probe light for optical absorption measurements was provided by the microscope's 100 W tungsten-halogen lamp and 0.3 NA condenser optics. A visible bandpass filter (Schott: BG40) and OD 9 neutral density filter was placed between the lamp and the condenser to reduce the thermal load on the sample and cryostat.

To induce photoisomerization, the crystal was illuminated with 505 nm light from a ThorLabs M505F1 fiber optically coupled light-emitting diode (LED). The light from the LED was collimated and then coupled into the microscope through a side port, focusing it onto the back aperture of the objective, thus filling the field of view and evenly illuminating the entire crystal. The excitation power measured at the objective was typically 370 μ W giving an estimated 340 μ W illuminating the field of view.

Optical absorption spectra were recorded by imaging the crystal on the entrance slit (75 μ m) of the spectrometer and dispersing the light, using a 150 line/mm grating, onto the detector. The image was positioned such that 30 rows of the detector were illuminated with light that passed through the crystal (I_T), whereas 30 rows of the detector directly above the crystal recorded light that passed through only the sapphire substrate (I_0). Absorption spectra were then calculated as $-\log_{10}(I_T/I_0)$.

ASSOCIATED CONTENT

S Supporting Information

The Supporting Information is available free of charge on the ACS Publications website at DOI: 10.1021/acs.chemmater.9b01738.

Movie associated with Figure 2 showing cycle 1 of light-induced photoisomerization process and thermal recovery of the main subject crystal to its dark state (MOV) Movie associated with Figure 3 (top panel) showing cycle 2 of light-induced photoisomerization process and thermal recovery of the main subject crystal to its dark state (MOV)

Movie associated with Fgiure 3 (bottom panel)-showing cycle 3 of light-induced photoisomerization process and thermal recovery of the main subject crystal to its dark state (MOV)

Analogous movie that demonstrates reproducibility of the peeling effect via a second crystal that undergoes cycle 1 of light-induction and warming (MOV)

Analogous movie that demonstrates reproducibility of the peeling effect via a second crystal that undergoes cycle 2 of light-induction and warming (MOV)

Analogous movie that demonstrates reproducibility of the peeling effect via a second crystal that undergoes cycle 3 of light-induction and warming (MOV) Movie of the original crystal undergoing a fourth cycle of light-induction and warming, 6 months after cycles 1-3 (MOV)

Crystal structure refinement details, especially those associated with the twinning and disorder of 1 (PDF) X-ray crystallographic data for 1 in its dark state (CIF) X-ray crystallographic data for 1 in its dark- and light-induced states (CIF)

X-ray crystallographic data for 1 in its dark- and light-induced state (non-twinned refinement) (CIF)

AUTHOR INFORMATION

Corresponding Author

*E-mail: jmc61@cam.ac.uk.

OBCID (

Jacqueline M. Cole: 0000-0002-1552-8743 David J. Gosztola: 0000-0003-2674-1379

Author Contributions

J.M.C. performed all of the photocrystallography, optical microscopy, and absorption spectroscopy work, with experimental assistance from S.G.W. and Y.-S.C. in beamline operation at the synchrotron and D.J.G. in setting up the optical microscopy and absorption spectroscopy apparatus. J.M.C. was the Ph.D. supervisor of J.d.J.V.-G. who synthesized the material. J.M.C. drafted the manuscript, which was written through contributions of all authors.

Notes

The authors declare no competing financial interest.

ACKNOWLEDGMENTS

J.M.C. thanks the 1851 Royal Commission of the Great Exhibition for the 2014 Fellowship in Design, hosted by Argonne National Laboratory where work done was supported by the U.S. Department of Energy (DOE) Office of Science, Office of Basic Energy Sciences, and used research resources of the Center of Nanoscale Materials and the Advanced Photon

Source (APS), Office of Science User Facilities operated for the DOE Office of Science by Argonne National Laboratory, supported by the U.S. DOE, all under contract no. DE-AC02-06CH11357. Within the APS, NSF's ChemMatCARS Sector 15 is principally supported by the Divisions of Chemistry (CHE) and Materials Research (DMR), National Science Foundation, under grant nos. NSF/CHE-1346572 and NSF/ CHE-1834750. Use of the PILATUS3 X CdTe 1M detector is supported by the National Science Foundation under grant no. NSF/DMR-1531283. J.M.C. is indebted to the BASF/Royal Academy of Engineering Senior Research Fellowship in Data-Driven Molecular Engineering of Functional Materials, and the ISIS Facility, STFC Rutherford Appleton Laboratory, UK, for financial support. J.d.J.V.-G. acknowledges the National Council of Science and Technology of Mexico (CONACyT) and the Cambridge Trust for a Ph.D. Scholarship (217553).

■ REFERENCES

- (1) Abendroth, J. M.; Bushuyev, O. S.; Weiss, P. S.; Barrett, C. J. Controlling Motion at the Nanoscale: Rise of the Molecular Machines. *ACS Nano* **2015**, *9*, 7746–7768.
- (2) Midolo, L.; Schliesser, A.; Fiore, A. Nano-opto-electromechanical Systems. *Nat. Nanotechnol.* **2018**, *13*, 11–18.
- (3) Bochmann, J.; Vainsencher, A.; Awschalom, D. D.; Cleland, A. N. Nanomechanical Coupling between Microwave and Optical Photons. *Nat. Phys.* **2013**, *9*, 712–716.
- (4) Naumov, P.; Chizhik, S.; Panda, M. K.; Nath, N. K.; Boldyreva, E. Mechanically Responsive Molecular Crystals. *Chem. Rev.* **2015**, 115, 12440–12490.
- (5) Zhu, L.; Al-Kaysi, R. O.; Bardeen, C. J. Photoinduced Ratchet-like Rotational Motion of Branched Molecular Crystals. *Angew. Chem., Int. Ed.* **2016**, *55*, 7073–7076.
- (6) Kim, K.; Al-Muhanna, M. K.; Al-Suwaidan, S. D.; Al-Kaysi, R. O.; Bardeen, C. J. Photoinduced Curling of Organic Molecular Crystal Nanowires. *Angew. Chem.* **2013**, *125*, 7027–7031 and ; *Angew. Chem., Int. Ed.* **2013**, *27*, 6889–6893.
- (7) Koshima, H.; Ojima, N.; Uchimoto, H. Mechanical Motion of Azobenzene Crystals upon Photoirradiation. *J. Am. Chem. Soc.* **2009**, 131, 6890–6891.
- (8) Bushuyev, O. S.; Singleton, T. A.; Barrett, C. J. Fast, Reversible, and General Photomechanical Motion in Single Crystals of Various Azo Compounds using Visible Light. *Adv. Mater.* **2013**, *25*, 1796–1800
- (9) Colombier, I.; Spagnoli, S.; Corval, A.; Baldeck, P. L.; Giraud, M.; Leaustic, A.; Yu, P.; Irie, M. Diarylethene Microcrystals make Directional Jumps upon Ultraviolet Irradiation. *J. Chem. Phys.* **2007**, *126*, 011101–011101.
- (10) Medishetty, R.; Husain, A.; Bai, Z.; Runcevski, T.; Dinnebier, R. E.; Naumov, P.; Vittal, J. J. Single Crystals Popping under UV light: the First Example of a Photosalient Effect Triggered by a [2 + 2] Cycloaddition Reaction. *Angew. Chem., Int. Ed.* **2014**, *53*, 5907–5911.
- (11) Natarajan, A.; Tsai, C. K.; Khan, S. I.; McCarren, P.; Garcia-Garibay, M. A. The Photoarrangement of h-Santonin is a Single-crystal-to-single-crystal Reaction: a Long kept Secret in Solid-state Organic Chemistry Revealed. *J. Am. Chem. Soc.* **2007**, *129*, 9846–9847.
- (12) Tong, F.; Al-Haidar, M.; Zhu, L.; Al-Kaysi, R. O.; Bardeen, C. J. Photoinduced Peeling of Molecular Crystals. *Chem. Commun.* **2019**, *55*, 3709–3712.
- (13) Ashcroft, C. M.; Cole, J. M. Molecular Engineering of Organic and Organometallic Second-order Nonlinear Optical Materials. In *Handbook of Organic Materials for Electronic and Photonic Devices*, 2nd ed.; Ostroverkhova, O., Ed.; Woodhead Publishing: Cambridge, 2019; p 152.
- (14) Coppens, P.; Novozhilova, I.; Kovalevsky, A. Photoinduced Linkage Isomers of Transition-metal Nitrosyl Compounds and Related Complexes. *Chem. Rev.* **2002**, *102*, 861–884.

(15) Masciocchi, N.; Kolyshev, A. N.; Dulepov, V. E.; Boldyreva, E. V.; Sironi, A. Study of the Linkage Isomerization $[Co(NH_3)_5NO_2]$ -Br₂ <= > $[Co(NH_3)_5ONO]$ Br₂ in the Solid State by X-ray Powder Diffraction. *Inorg. Chem.* **1994**, 33, 2579–2585.

- (16) Naumov, P.; Sahoo, S. C.; Zakharov, B. A.; Boldyreva, E. V. Dynamic Single Crystals: Kinematic Analysis of Photoinduced Crystal Jumping (the Photosalient Effect). *Angew. Chem., Int. Ed.* **2013**, *52*, 9990–9995.
- (17) Coppens, P.; Fomitchev, D. V.; Carducci, M. D.; Culp, K. Crystallography of Molecular Excited States: Transition Metal Nitrosyl Complexes and the Study of Transient Species. *J. Chem. Soc., Dalton Trans.* 1998, 6, 865–872.
- (18) Cole, J. M. Single-crystal X-ray Diffraction Studies of Photo-induced Molecular Species. *Chem. Soc. Rev.* **2004**, *33*, 501–513.
- (19) Cole, J. M. Photocrystallography. Acta Crystallogr., Sect. A: Found. Crystallogr. 2008, 64, 259–271.
- (20) Cole, J. M. A New Form of Analytical Chemistry: Distinguishing the Molecular Structure of Photo-induced States from Ground-states. *Analyst* **2011**, *136*, 448–455.
- (21) Kovalevsky, A. Y.; Bagley, K. A.; Coppens, P. The first Photocrystallographic Evidence for Light-induced Metastable Linkage Isomers of Ruthenium Sulfur Dioxide Complexes. *J. Am. Chem. Soc.* **2002**, *124*, 9241–9248.
- (22) Kovalevsky, A. Y.; Bagley, K. A.; Cole, J. M.; Coppens, P. Light-induced Metastable Linkage Isomers of Ruthenium Sulfur Dioxide Complexes. *Inorg. Chem.* **2003**, *42*, 140–147.
- (23) Bowes, K. F.; Cole, J. M.; Husheer, S. L. G.; Raithby, P. R.; Savarese, T. L.; Sparkes, H. A.; Teat, S. J.; Warren, J. E. Photocrystallographic Structure Determination of a new Geometric Isomer of $[Ru(NH_3)_4(H_2O)(\eta^1\text{-OSO})][MeC_6H_4SO_3]_2$. Chem. Commun. **2006**, 2448–2450.
- (24) Phillips, A. E.; Cole, J. M.; d'Almeida, T.; Low, K. S. Effects of the Reaction Cavity on Metastable Optical Excitation in Ruthenium-sulfur Dioxide Complexes. *Phys. Rev. B: Condens. Matter Mater. Phys.* **2010**, 82, 155118.
- (25) Phillips, A. E.; Cole, J. M.; d'Almeida, T.; Low, K. S. Ru-OSO Coordination Photogenerated at 100 K in Tetraammineaqua (sulfur dioxide) ruthenium (II)(±) Camphorsulfonate. *Inorg. Chem.* **2012**, *51*, 1204–1206.
- (26) Sylvester, S. O.; Cole, J. M.; Waddell, P. G. Photoconversion Bonding Mechanism in Ruthenium Sulfur Dioxide Linkage Photoisomers Revealed by In Situ Diffraction. *J. Am. Chem. Soc.* **2012**, *134*, 11860–11863.
- (27) Sylvester, S. O.; Cole, J. M. Solar-powered Nanomechanical Transduction from Crystalline Molecular Rotors. *Adv. Mater.* **2013**, 25, 3324–3328.
- (28) Sylvester, S. O.; Cole, J. M. Quantifying Crystallographically Independent Optical Switching Dynamics in Ru SO_2 Photoisomers via Lock-and-key Crystalline Environment. *J. Phys. Chem. Lett.* **2013**, 4, 3221–3226.
- (29) Sylvester, S. O.; Cole, J. M.; Waddell, P. G.; Nowell, H.; Wilson, C. SO_2 Phototriggered Crystalline Nanomechanical Transduction of Aromatic Rotors in Tosylates: Rationalization via Photocrystallography of $[Ru(NH_3)_4SO_2X]$ tosylate $_2$ (X = pyridine, 3-Cl-pyridine, 4-Cl-pyridine). *J. Phys. Chem. C* **2014**, *118*, 16003–16010.
- (30) Chemicalize was used for prediction of pK_a values, https://chemicalize.com/; accessed April 2019, developed by ChemAxon (http://www.chemaxon.com).
- (31) Jacobsen, R. S.; Andersen, K. N.; Borel, P. I.; Fage-Pedersen, J.; Frandsen, L. H.; Hansen, O.; Kristensen, M.; Lavrinenko, A. V.; Moulin, G.; Ou, H.; Peucheret, C.; Zsigri, B.; Bjarklev, A. Strained Silicon as a new Electro-optic Material. *Nature* **2006**, *441*, 199–202.
- (32) Pustogow, A.; McLeod, A. S.; Saito, Y.; Basov, D. N.; Dressel, M. Internal Strain Tunes Electronic Correlations on the Nanoscale. *Sci. Adv.* **2018**, *4*, No. eaau9123.
- (33) Lynch, S. M.; Shelbyy, J. Crystal Clamping in Lead Titanate Glass-Ceramics. J. Am. Ceram. Soc. 2006, 67, 424–427.

- (34) Liu, G.; Liu, J.; Ye, X.; Nie, L.; Gu, P.; Tao, X.; Zhang, Q. Self-Healing Behavior in a Thermo-Mechanically Responsive Cocrystal during a Reversible Phase Transition. *Angew. Chem., Int. Ed.* **2017**, *56*, 198–202.
- (35) Gupta, P.; Karothu, D. P.; Ahmed, E.; Naumov, P.; Nath, N. K. Thermally Twistable, Photobendable, Elastically Deformable, and Self-Healable Soft Crystals. *Angew. Chem., Int. Ed.* **2018**, *57*, 8498–8502
- (36) Karothu, D. P.; Weston, J.; Desta, I. T.; Naumov, P. Shape-Memory and Self-Healing Effects in Mechanosalient Molecular Crystals. *J. Am. Chem. Soc.* **2016**, *138*, 13298–13306.
- (37) Worthy, A.; Grosjean, A.; Pfrunder, M. C.; Xu, Y.; Yan, C.; Edwards, G.; Clegg, J. K.; McMurtrie, J. C. Atomic Resolution of Structural Changes in Elastic Crystals of Copper(II) Acetylacetonate. *Nat. Chem.* **2018**, *10*, 65–69.
- (38) Panda, M. K.; Ghosh, S.; Yasuda, N.; Moriwaki, T.; Mukherjee, G. D.; Reddy, C. M.; Naumov, P. Spatially Resolved Analysis of Short-Range Structure Perturbations in a Plastically Bent Molecular Crystal. *Nat. Chem.* **2015**, *7*, 65–72.